Journal of Sol-Gel Science and Technology
https://doi.org/10.1007/s10971-023-06131-9

INVITED PAPER: INDUSTRIAL AND TECHNOLOGICAL APPLICATIONS OF SOL-GEL AND HYBRID MATERIALS

Upscaling TiO_2 sol-gel technology to make it a competitive way for coating manufacture and processing at an industrial scale

Benoît Heinrichs[1] · Stéphanie D. Lambert[1] · Géraldine Léonard[1,2] · Christelle Alié[1] · Sigrid Douven[1,3] · Joachim Caucheteux[1] · Jérémy Geens[1] · Alain Daniel[4] · Catherine Archambeau[4] · Christelle Vreuls[5] · Alain Devos[6] · Frédéric Luizi[7] · Julien G. Mahy[1,8]

Received: 8 December 2022 / Accepted: 30 April 2023

Abstract

In this work, an eco-friendly sol-gel synthesis of pure and doped TiO_2, previously developed at lab-scale, is applied in three different environmental applications at lab-scale and then, upscaled towards industrial applications. For each application, the TiO_2 is used as a coating deposited mainly on steel substrates. The three applications are: (i) the development of a photocatalytic reactor made of a UV lamp, an ozonation part and a TiO_2 photocatalytic coating to treat water from swimming pools, (ii) the development of a new generation of low energy sterilizers by an advanced oxidation process using a photocatalytic coating illuminated by a blue LED, and (iii) an easy-to-clean coating for outdoor steel. In each application, the up-scale results were similar to those obtained in the laboratory with respect to the crystallinity, the visual aspect, the hydrophilicity, and the photocatalytic properties of the produced coatings. These developments showed the possibility to bring sol-gel TiO_2 products outside the laboratory towards pilot and industrial applications, and opens the way for many possible up-scaled sol-gel based environmental applications.

Supplementary information The online version contains supplementary material available at https://doi.org/10.1007/s10971-023-06131-9.

✉ Julien G. Mahy
julien.mahy@uliege.be

[1] Department of Chemical Engineering – Nanomaterials, Catalysis & Electrochemistry, University of Liège, B6a, Quartier Agora, Allée du six Août 11, 4000 Liège, Belgium

[2] Carmeuse, Rue du Château 13, 5300 Andenne, Belgium

[3] SWDE, Rue de la concorde 41, 4800 Verviers, Belgium

[4] AC&CS – CRM GROUP, B57, Quartier Polytech 3, Allée de l'Innovation 1, 4000 Liège, Belgium

[5] Environmental Department, Celabor, Research Centre, Herve, Belgium

[6] Mecanic Systems, Avenue de l'Artisanat 12b, 1420 Braine-l'Alleud, Belgium

[7] Aquatic Science S.A., Zoning des Hauts Sarts, 3ème avenue 1, 4040 Herstal, Belgium

[8] Institut National de la Recherche Scientifique (INRS), Centre-Eau Terre Environnement, Université du Québec, 490, Rue de la Couronne, Québec, QC G1K 9A9, Canada

Published online: 12 May 2023

Graphical Abstract

An eco-friendly sol-gel synthesis of pure and doped TiO_2, previously developed at lab-scale, is applied in three different environmental applications at lab-scale and then, successfully upscaled towards industrial applications.

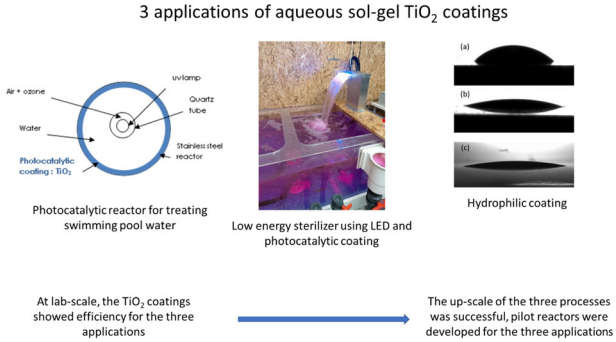

Keywords Advanced oxidation process · Application of Sol-Gel technology · Hydrophilicity · Visible absorption · Pollutant degradation · TiO_2 thin film

Highlights

- Eco-friendly sol-gel synthesis of pure and doped TiO_2 developed for industrial applications.
- TiO_2 is deposited on steel substrates for three applications.
- TiO_2 coatings used for decontamination of swimming pool and fountain waters.
- TiO_2 layer also used as easy-to-clean coating for outdoor pre-painted steel.
- The efficiency of the layers is successfully up-scaled from laboratory to industrial applications.

1 Introduction

Since the 1930s, the sol-gel process has been used to produce numerous metal oxides [1]. This process occurs under soft conditions, *i.e.* at low temperature and pressure. This process involves the formation of a sol followed by the formation of a gel, giving its name. A sol is a suspension of solid particles in a liquid, the sizes of which range from nanometers to micrometers [1]. The two main reactions are hydrolysis and the condensation of matrix precursors. By controlling the rates of these reactions, a liquid sol or a solid gel can be obtained, depending on the desired application [1].

Sol-Gel chemistry allows amorphous or crystalline materials to be obtained, with low or high porosity depending on the needs of the application [2–9]. Sol-gel technology can be used for a large range of applications because it is also possible to combine organic species and mineral species very easily. This gives the advantage of enabling the incorporation of organic homogeneous catalysts in a porous matrix for example [10–12]. Sol-gel processing allows either powders or thin films to be obtained [13–17]. This is also an advantage because the same material can be used under different forms to take advantage of, for example, the textural properties for adsorption in powders or to immobilize a catalyst on an oxide film.

Sol-gel processing has been also used for environmental applications, often to produce materials that can be implemented in depollution [18, 19]. Many metallic oxides that can be prepared by sol-gel processing are semiconductors such as TiO_2 [20–23], ZnO [24–27], SnO_2 [28–30], or MnO_2 [31, 32]. These materials can be used as photocatalyst to degrade organic pollutants. Indeed, photocatalysis allows the production of highly reactive species, involving the use of an appropriate photocatalyst and light that can react and decompose organic molecules, in the best case to form CO_2 and H_2O as final decomposition products [33, 34]. The most commonly used photocatalyst is titanium dioxide (TiO_2) [35–37] and many lab-scale applications for water and air depollution have been developed with sol-gel processes. Nevertheless, only a few studies report works that have been transferred from the laboratory towards pilot or industrial scale application. Indeed, to up-scale a lab-scale process, many steps are usually needed: the synthesis must be feasible and compatible with up-scaling by using compounds with the lowest toxicity and under soft synthesis conditions; the shaping of the material must be made with industrial techniques such as roll-coating or spray-coating, for example, for coating deposition; and the properties of the up-scaled products must be comparable to those prepared on a the lab-scale. The sol-gel process seems still quite well adapted to up-scaling due

its high versatility in its synthesis conditions and resulting material shapes.

As indicated previously, the most widely used photocatalyst is TiO_2 [35–37], which is a sensitive semiconductor to UV radiation and inexpensive [38]. TiO_2 exists in three different crystallographic structures: anatase (band gap of 3.2 eV), brookite (band gap > 3.2 eV), and rutile (band gap of 3.0 eV) [39]. The best phase for a photocatalytic application is the anatase phase [39]. Numerous dopants have been developed to extend its absorption spectrum in the visible range [40–44]. Among those dopants, iron and nitrogen are quite efficient for increasing the activity of TiO_2 in the visible range and have many advantages such as being non-toxic, inexpensive, widely available, and efficient for extending the photocatalytic activity of TiO_2 into the visible range [44, 45].

Coatings of TiO_2 prepared at lab-scale have shown very good photocatalytic properties for pollutant degradation in water [46–48] and air [49, 50], but present also excellent hydrophilic properties [47, 51].

In this work, an eco-friendly sol-gel synthesis of pure and Fe/N doped TiO_2, previously developed at lab-scale [45, 52], is applied in three different environmental applications via three different research projects and then upscaled towards industrial applications. For each application, TiO_2 is used as a coating deposited mainly on steel. The paper will detail the goals of each project, the lab-scale results and the resulting upscaled application with a comparison with the lab-scale products. The three projects are: (i) the UVozone project, which developed a photocatalytic reactor involving UV irradiation, ozone and a TiO_2 photocatalytic coating to treat water from swimming pools, (ii) the BlueV project, which developed a new generation of low energy sterilizers involving an advanced oxidation process using a photocatalytic coating illuminated by a LED, and (iii) the DAO project, which developed easy-to-clean coatings for outdoor steel. The novelty of this study resides in the extrapolation of three different environmental processes using sol-gel TiO_2 materials developed at laboratory scale to larger scale and even to a commercial-scale photocatalytic reactor.

2 Materials and Methods

2.1 Organic TiO_2 synthesis

8 mL of titanium isopropoxide (>97%, Sigma-Aldrich) was mixed for 30 min in 48 mL of 2-methoxyethanol (>99%, Sigma-Aldrich) in a closed vessel. In another vessel, 1.2 mL of deionized water was mixed with 48 mL of 2-methoxyethanol. Then, the second vessel was added to the first and mixed for 1 h. The sol was then ready for deposition. This suspension is called organic TiO_2. All operations were made in a glovebox under a N_2 atmosphere.

2.2 Aqueous TiO_2 synthesis

250 mL of distilled water was acidified to a pH of 1 with HNO_3 (65%, Merck). 5 mL of titanium isopropoxide was mixed with 15 mL of isopropanol (99.5%, Acros) for 15 min. Then the second solution was mixed in the first and the resulting mixture was then heated at 80 °C for 4 h. The resulting suspension is called aqueous TiO_2. 20 mL of the resulting suspension was also dried under ambient air to obtain the corresponding powder that can be more easily characterized than the film in some cases.

2.3 Aqueous doped TiO_2 synthesis

Ferric nitrate ($Fe(NO_3)_3{\cdot}9H_2O$, Merck) and ammonium chloride (NH_4Cl, UCB, Leuven, Belgium) were mixed in 250 mL of distilled water which was then acidified to a pH of 1. In a second vessel, 5 mL of titanium isopropoxide was mixed with 15 mL of isopropanol for 15 min. Then the second solution was mixed with the first and the resulting mixture was then heated at 80 °C for 4 h. The resulting suspension is called doped TiO_2. 20 mL of the resulting suspension was also dried under ambient air to obtain the corresponding powder that can be more easily characterized than the film in some cases.

2.4 Large scale TiO_2 synthesis

Large scale synthesis of the aqueous TiO_2 sol was undertaken in a 5 L glass batch reactor with a water heating envelop. In this case, 3.6 L of distilled water was acidified to a pH of 1. In a second vessel, 500 mL of titanium isopropoxide was mixed with 215 mL of isopropanol. Then the second solution was mixed with the first in the glass reactor with heating at 80 °C for 4 h. The resulting suspension is called large-scale TiO_2. 20 mL of the resulting suspension was also dried under ambient air to obtain the corresponding powder that can be more easily characterized than the film in some cases.

2.5 Deposition methods

2.5.1 Substrates

This section gives all the information about the different substrates used for coatings.

(i) Stainless steel slides (316 L steel), of dimensions 2.5 cm × 7.5 cm × 0.7 mm or 21 cm × 15 cm x 0.7 cm, with or without a white painted layer.

(ii) Steel cylinder (316 L) with a diameter and length of 10 cm. The steel reactor is illustrated in Fig. S1.

(iii) Glass slide (Marienfeld Superior) of dimensions 25 mm × 75 mm × 1 mm.

(iv) Quartz tube of diameter 3 cm and 7 cm in height.

2.5.2 Coating deposition methods

2.5.2.1 Dip-coating The substrates were thoroughly cleaned before coating. The speed of withdrawal of the slide from the solution during the dip coating operation was 60 mm/min, as optimized by Malengreaux et al. [53] for this type of TiO_2 synthesis. Films were dried at 100 °C for 30 s and kept in the dark.

2.5.2.2 Bar-coating The substrate was treated with 2 M HNO_3 solution to increase film adhesion by steel passivation [54]. Then, the TiO_2 sol was deposited on the steel by bar-coating with an Elcometer 4340 Automatic Film Applicator with a bar-speed of 1 cm/s. The films were dried at 100 °C for 30 s and kept in the dark.

2.5.2.3 Continuous roll-to-roll deposition This deposition method was made on a pilot line detailed in [52]. The steel substrate was 25 cm wide, and the band length was 800 m. The experiment was carried out on a pilot line equipped with an unwinder, a cleaning section, a roll-coater, an inductor for solvent evaporation, an air cooler and a rewinder [52]. The cleaning section was composed of a degreasing bath to remove dirt and an acidic bath (2 M HNO_3 solution) to increase the film adhesion by steel passivation [54]. The temperature reached by the strip in the inductor section was 100 °C. The coating can be deposited at line speed ranging from 30 to 120 m/min, allowing the amount of TiO_2 deposited to be adapted. Typically, the samples analysed in this paper were deposited at 60 m/min.

2.5.2.4 Pump-coating the cylindrical substrate was filled with the suspension and then the liquid was removed using a peristaltic pump at a speed of 60 mm/min connected to a plastic tube immersed in the liquid.

2.5.2.5 Turn-coating The cylindrical substrate was rolled into a basin where there was only 1 cm of floor height (Fig. S2). The part was rolled manually for 5 min to also approach a speed of 60 mm/min along the walls which emerge from the solution.

For the 1 m reactor, the suspension was put inside the reactor, its extremities were sealed, then it was fixed on a mechanical lathe rotating at 60 mm/min (Fig. S3). After ten tours, the excess liquid was removed, and the reactor was dried by rotating with the extremities opened.

2.5.2.6 Spray-coating This technique consisted of spraying the TiO_2 suspensions onto the surface of the samples which were placed on a hotplate at 60 °C (Fig. S4). The spray was placed at a distance of 7 cm from the surface to deposit the coating on the sample for a defined number of time (5 times). A drying step at 80 °C of 5 min was introduced after these five passes. This procedure (5 layers + drying) was repeated several times (see Upscaled application). At the end of the deposition, the samples were dried at 80 °C for 5 min.

2.6 Characterization

The crystallographic properties were determined using X-Ray diffraction (XRD). The powder patterns were recorded with a Bruker D8 Twin-Twin powder diffractometer using Cu-K_α radiation. The crystallinity of the films was characterized by grazing incidence X-ray diffraction (GIXRD) in a Bruker D8 diffractometer using Cu-K_α radiation and operating at 40 kV and 40 mA. The incidence beam angle was 0.25°.

The film thickness was estimated by profilometry (Veeco Dektak 8 Stylus Profiler, Bruker), noting that this technique can only be applied if the roughness of the substrate is smaller than the thickness of the deposited film.

The film adhesion was tested by rubbing the surface with a dry and a wet cloth, by flowing water or ethanol at the surface or by ICP-AES analysis of the Ti content in water where samples were immersed under stirring.

The hydrophilicity of films was measured by the wet contact angle measurement technique on a DGD fast/60 goniometer device by deposition of a 10 µL water drop on the film. The contact angle was measured one day after film deposition, with the coated sample stored in the dark. The measurement was performed three times to assess reproducibility.

UV/visible diffuse reflectance spectra of pure and doped aqueous TiO_2 powders were measured on a Perkin Elmer Lambda 1050 S UV/VIS/NIR spectrophotometer, equipped with a spectralon coated integrating sphere (150 mm InGaAs Int. Sphere from PerkinElmer).

The pure and doped aqueous TiO_2 powders were observed by transmission electron microscopy (TEM) using a Phillips CM 100 TEM with an accelerating voltage of 200 kV.

SEM images were obtained on a field-emission JEOL 7600 F scanning electron microscope operating at 15 kV.

2.7 Photocatalytic experiments

2.7.1 Methylene Blue degradation under UV-A (lab-scale)

The photocatalytic activity of TiO_2 films was evaluated by monitoring the degradation of methylene blue (MB) under ultraviolet light (Osram Sylvania, Blacklight-Bleu

Lamp, F 18 W/BLB-T8) over 6 h [52]. The spectra of the lamps were measured with a Mini-Spectrometer TM-UV/vis C10082MD from Hamamatsu. UV-A light can be considered as monochromatic with a wavelength $\lambda = 365$ nm. Each film was placed in a petri dish with 25 mL of 2×10^{-5} M of MB solution [52]. The degradation of MB was evaluated from absorbance measurements with a Genesys 10 S UV-Vis spectrophotometer (Thermo Scientific) at $\lambda = 665$ nm. Preliminary adsorption tests performed in the dark (dark tests) showed that MB was not adsorbed on the surface. A blank test, consisting of irradiating the pollutant solution for 24 h in a petri dish without any catalyst, showed that MB concentration under UV-A illumination remains unchanged. The petri dishes with catalysts and pollutant were stirred on orbital shakers and illuminated for 6 h. Aliquots of MB were sampled at the beginning and after 6 h. Each photocatalytic measurement was replicated three times to assess the reproducibility of the data [52].

2.7.2 Methylene Blue degradation under UV lamp (large scale with UVozone reactor)

The photocatalytic activity of the TiO_2 film deposited in the UVozone reactor was evaluated by monitoring the degradation of MB under ultraviolet light (lamp spectrum given in Fig. S5) over 2 h. The installation (Fig. S6) consisted of a basin containing a solution of MB (2×10^{-5} mol/L). This solution was sucked into pipes by a pump that circulates the liquid. This was injected into the bottom of the UVozone reactor and flowed into the device. Finally, having arrived at the top of the device, the liquid was directed towards the initial basin. An air suction system was developed using the creation of a vacuum (venturi effect). The air was thus sucked in from the bottom of the UVozone, travelled upwards throughout the UVozone being converted into ozone, and was then injected into the pipe containing the MB solution. 25 mL was sampled every 15 min at the location indicated by the orange arrow of Fig. S6; the injection of ozone began only after 1 h of experimentation. The degradation of MB was evaluated from absorbance measurements with a Genesys 10 S UV-Vis spectrophotometer (Thermo Scientific) at $\lambda = 665$ nm.

2.7.3 Para-nitrophenol and Rhodamine B degradation under visible LED light (lab-scale)

The photocatalytic activity of TiO_2 films was evaluated (i) by monitoring the degradation of *p*-nitrophenol (PNP) and (ii) by monitoring the degradation of rhodamine B (RB) under visible LED light (LED Würth Elektronic WL-SUMW SMT Ultraviolet Ceramic Waterclear, Würth Elektronik GmbH & Co. KG, Waldenburg, Germany) in two similar photocatalytic experiments [45].

The spectrum of the lamp was measured with a Mini-Spectrometer TM-UV/vis C10082MD from Hamamatsu. The LED light can be considered as quasi monochromatic with a wavelength of 395 nm [45].

The experimental procedure was very similar for both pollutants. Indeed, each coated steel slide was placed in a Petri dish with 25 mL of PNP solution (10^{-4} mol/L) or RB solution (2.5×10^{-6} mol/L). The Petri dish was closed with a lid in order to avoid evaporation. The degradation of PNP or RB was evaluated from absorbance measurements with a Genesys 10 S UV-Vis spectrophotometer (Thermo Scientific, Waltham, MA, USA) at 317 nm or 554 nm, respectively [45]. Adsorption tests were performed in the dark (dark tests) to determine whether PNP or RB was adsorbed by the films or the substrates. Blank tests, consisting of irradiating the pollutant solution in a Petri dish without any catalyst or support, were carried out to estimate the decomposition of PNP or RB under the corresponding light [45]. The Petri dishes with catalyst and pollutant were stirred on orbital shakers at 80 rpm. Aliquots of PNP or RB were sampled throughout the experiment and put back in the Petri dishes after absorbance measurements to keep the volume constant. The photocatalytic degradation is equal to the total degradation of PNP or RB taking the catalyst adsorption (dark test) into account. Each photocatalytic measurement was triplicated to assess the reproducibility of the data [45].

2.7.4 Rhodamine B degradation under LED light (large scale with pilot fountain)

The photocatalytic activity of the pilot fountain was evaluated by monitoring the degradation of RB under visible LED light (LED Würth Elektronic WL-SUMW SMT Ultraviolet Ceramic Waterclear, Würth Elektronik GmbH & Co. KG, Waldenburg, Germany). A 5 m³/h pump was immersed in the 1.5 m³ transparent tank and connected to the fountain prototype (see Fig. S7). The degradation of RB was evaluated from absorbance measurements with a Genesys 10 S UV-Vis spectrophotometer (Thermo Scientific, Waltham, MA, USA) at 554 nm with sampling every hour.

3 Results and discussions

Three applications of TiO_2 material synthesized by aqueous sol-gel process will be detailed in this part. For each application, lab-scale results will be discussed then the up-scaled application will be detailed.

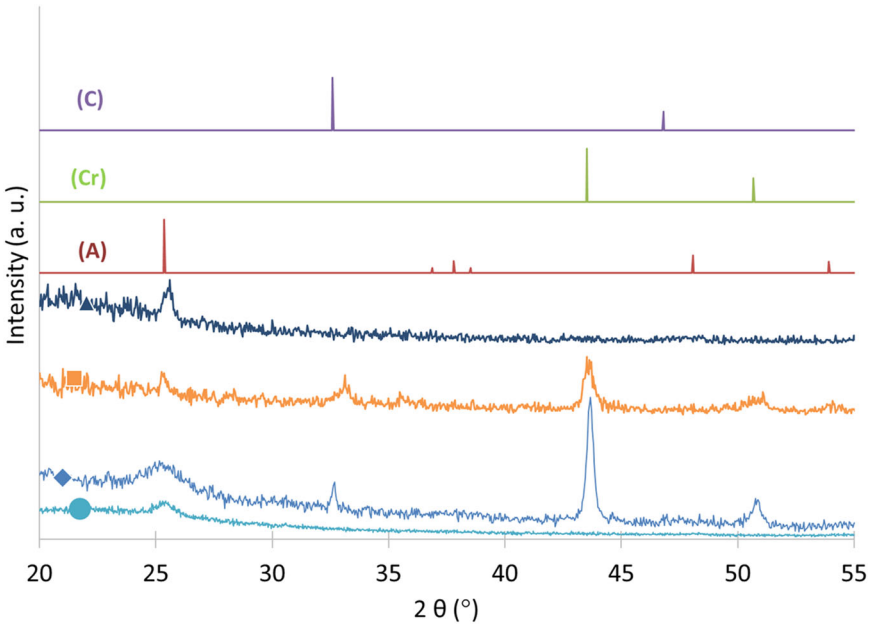

Fig. 1 Grazing incidence X-ray diffraction (GIXRD) patterns of the TiO_2 coatings on the different substrates: (●) aqueous TiO_2 on quartz, (♦) aqueous TiO_2 on steel, (■) organic TiO_2 on steel, and (▲) organic TiO_2 on quartz. (A) Reference pattern of anatase, (Cr) Reference pattern of iron chromium carbide, and (C) Reference pattern of chromium oxide

Table 1 Coating thickness measured by profilometry, TiO_2 released in water and MB photocatalytic degradation

Sample	$Thickness_{profilo}$ (nm) ± 5	$Thickness_{profilo}$ after adherence test (nm) ± 5	TiO_2 amount in water (mg/L)	MB degradation after 6 h (%) ± 5
Organic TiO_2 on quartz	15	16	< 0.01	27
Organic TiO_2 on Steel	–	–	< 0.01	15
Aqueous TiO_2 on quartz	18	20	< 0.01	22
Aqueous TiO_2 on steel	–	–	< 0.01	14

3.1 UVozone project

3.1.1 Goal of the project

The goal of this project is to develop a photocatalytic layer to coat the inside of a UV/ozone reactor made of a UV-Lamp inside a cylindrical metallic reactor where ozone and UV are used as bactericides to disinfect water from swimming pools. The intention is to have additional photocatalytic activity from this coating to enhance the efficiency of the process. Initially, photocatalytic layers will be developed and tested on a laboratory scale, then the best coating will be up-scaled. TiO_2 was chosen as photocatalytic material.

3.1.2 Laboratory scale

The organic and aqueous TiO_2 sols were explored at laboratory scale. These materials were deposited by dip-coating on quartz cylinders and on steel slides. Two substrates were used as the coating can be deposited on the inside of the steel reactor or on the quartz tube that surrounds the UV lamp.

Figure 1 shows the XRD patterns of the two coatings on both substrates. On both quartz and steel, anatase was obtained for both synthesis with the characteristic peak at 25° [52]. On steel substrate, some additional peaks are present which correspond to the steel substrate.

The thickness of the coating was estimated with profilometry (Table 1), but it was only possible on quartz substrate because the roughness of the steel is too high compared to the thickness of the deposit. For both syntheses on quartz, similar thickness was obtained of around 15–18 nm (Table 1). The adherence of the coatings was evaluated in two different experiments: (i) in a first one, different solvents were flowed across the surface of the coating then the thickness of the coating was measured, (ii) in a second one, the coating was immersed in water with constant stirring at 1200 rpm for 3 weeks, then the water was analyzed by ICP to check that no TiO_2 was detected and the coating thickness was remeasured by profilometry. As noted in Table 1, all samples passed both test as no

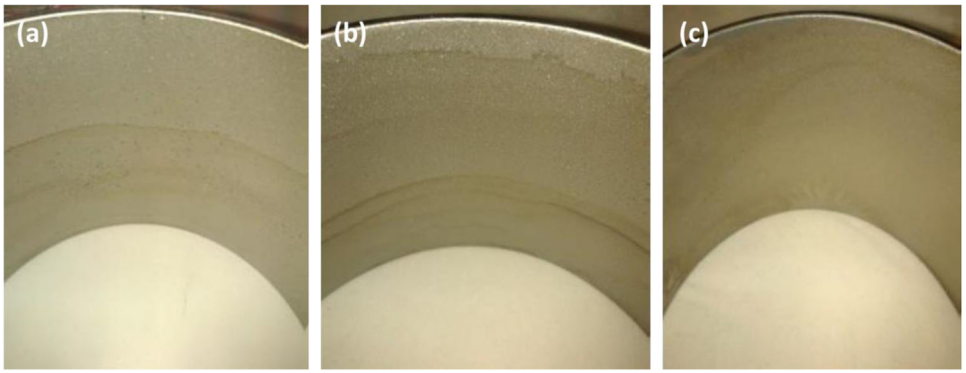

Fig. 2 Coating aspect after deposition: **a** Aqueous TiO_2 coating deposition on steel cylinder by dip-coating. **b** Aqueous TiO_2 coating deposition on steel cylinder by pump-coating. **c** Aqueous TiO_2 coating deposition on steel cylinder by turn-coating

difference in coating thickness was measured and no TiO_2 was detected by ICP.

The photocatalytic activity of the coating for MB degradation was evaluated under UV-A light (Table 1), with every coating leading to partial MB degradation after 6 h of illumination.

When the coating is deposited on the quartz substrate, the substrate absorbed a large amount of the UV radiation as can be observed in Fig. S5. Hence, less UV radiation was available for water disinfection if the coating was deposited on the quartz tube.

In order to choose the best coating for the application, some key parameters must be considered. First, concerning the photocatalytic properties, both coatings had similar properties with similar thickness. Nevertheless, concerning the synthesis, the aqueous TiO_2 is prepared with water as solvent, in contrast to the organic system which use 2-methoxyethanol as solvent. The aqueous synthesis occurred in ambient atmosphere while the organic TiO_2 synthesis is made in a glovebox under N_2 atmosphere. Finally, the organic route required calcination at 500 °C after deposition to obtain an anatase TiO_2 coating while the aqueous route yielded crystalline TiO_2 in suspension. The required calcination step in the former case damaged the steel and corroded it. To summarize, the most appropriate coating for this application was the aqueous TiO_2 material, which was chosen for the upscaled application. The coating was deposited on the inside of the steel vessel that composes the pilot reactor.

3.1.3 Upscaled application

To coat the inside of the steel reactor with TiO_2, first, smaller steel cylinders (10 × 10 cm) were used as substrate to determine to best deposition method. Three deposition methods were evaluated: (i) dip-coating, (ii) pump-coating, and (iii) turn-coating. For each method, the quality of the coating was evaluated by visual inspection, ease of deposition and adherence to choose the best method for deposition on the actual reactor vessel.

For the dip-coating, a similar process to that used for the steel slide was applied. The deposition on the cylinder appeared homogeneous (Fig. 2a), and the adherence of the coating in water, ethanol and acetone was stable upon visual inspection. The main issue for this deposition method is that a large volume of suspension is needed for deposition on the large surface of the pilot reactor (several liters), with the entire piece being immersed in the liquid. Moreover, the coating is deposited also on the outside of the reactor, which consumes part of the suspension unnecessarily.

For the pump-coating, the principle is to fill the cylinder (with the extremity blocked) with the suspension to deposit the coating and then to remove it at a controlled speed using a peristaltic pump. The obtained coating is represented in Fig. 2b. The coating was less homogeneous than that obtained by dip-coating (Fig. 2a), but the coating was only deposited on the inside of the reactor. The adherence was also stable upon visual inspection in water, ethanol and acetone. In this case, a large amount of sol was also necessary to fill the cylinder for coating.

For the turn-coating, the cylinder was rotated in a basin containing 1 cm height of suspension. The produced coating is quite homogeneous (Fig. 2c) and had a stable adhesion upon visual inspection to the substrate after the experiments with water, ethanol and acetone. Moreover, this deposition method consumed only a small fraction of suspension. This deposition method was chosen to coat the pilot reactor.

The UVozone photocatalytic reactor to be coated is represented in Fig. S1. The deposit method used was a turn-coating adapted for the pilot reactor. Indeed, as shown in Fig. S3, the reactor was held with a turning axis which allowed control of the rotation speed; the TiO_2 suspension was then introduced in the reactor and its extremities were closed. After the rotation, the excess suspension was removed, and the coating was dried. Figure 3 shows the inside of the reactor before and after coating. Due to the size and shape of the reactor, the coating is difficult to characterize.

To ensure that a TiO_2 photocatalytic coating was present in the reactor and that it brings added value to the UVozone

reactor, a photocatalytic experiment was conducted on MB degradation (as described in Photocatalytic experiments). The evolution of the MB degradation is presented in Fig. 4, in blue when the TiO_2 coating was present and in red when only UV and ozone were applied (in both cases, the ozone was switched on after 60 min). It is clearly observed that the TiO_2 coating increased the rate of degradation of MB with around 10% more degradation after 120 min of experiments.

Moreover, experiments with water demonstrated that no leaching of TiO_2 occurred during operation.

Due to the efficiency of the photocatalytic coating, this reactor was commercialized by the society AQUATIC SCIENCE [55]. The optimized conditions (Table 2) for producing this reactor involve the use of an undoped aqueous TiO_2 sol which is deposited via turn-coating on the inside of the cylindrical steel reactor, followed by drying in ambient air by rotating the reactor with its extremities opened.

Fig. 3 Inside of the UVozone reactor before (left) and after (right) deposition of the aqueous TiO_2 coating

3.2 BlueV project

3.2.1 Goal of the project

The objective of the project is to develop a new generation of low energy sterilizers using advanced oxidation processes capable of advantageously replacing, in many uses, the current UV sterilizers. In this equipment, an emitter plate with an optimized wavelength (consisting of an LED emitting at 395 nm), will stimulate a nearby plate coated with TiO_2 photocatalytic paint aimed at disinfecting and decontaminating water. Due to the wavelength of the LED, the TiO_2 material must be doped to enhance its absorption spectrum. First, coatings at laboratory scale will be produced, characterized, and tested for the degradation of model pollutant. Then, larger substrate will be coated via spray coating and tested in larger photocatalytic experiments and introduced in a pilot fountain.

3.2.2 Laboratory scale

The synthesis chosen for producing the TiO_2 coating was based on the aqueous TiO_2 synthesis described in the

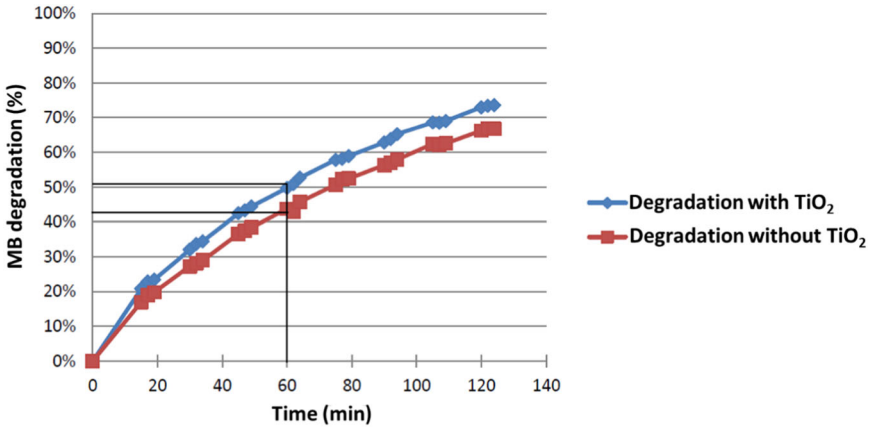

Fig. 4 MB degradation in large scale experiment: (blue) MB degradation with the TiO_2 coating and (red) MB degradation without the TiO_2 coating. The beginning of the ozonation is indicated by the black line at 60 min

Table 2 Summary of the large-scale results for the three applications (optimized conditions)

Large scale application	Deposited coating	Deposition condition	Substrate and size	Large scale application results
UVozone	Undoped aqueous TiO_2	Turn-coating at 60 mm/min followed by air drying	Steel cylindrical reactor of 1 m length	75% of MB degraded after 120 min of illumination under UV-A
BlueV	Fe/N doped aqueous TiO_2	Spray-coating (16 × 5 layers) followed by drying at 80 °C	Painted steel of 250 × 150 mm	65% of RB degraded after 72 h of illumination under visible LED
DAO	Undoped aqueous TiO_2	Roll-coating at 60 m/min followed by induction drying at 100 °C	Steel of 800 × 0.25 m	Water contact angle < 20° on the coating showing hydrophilic property

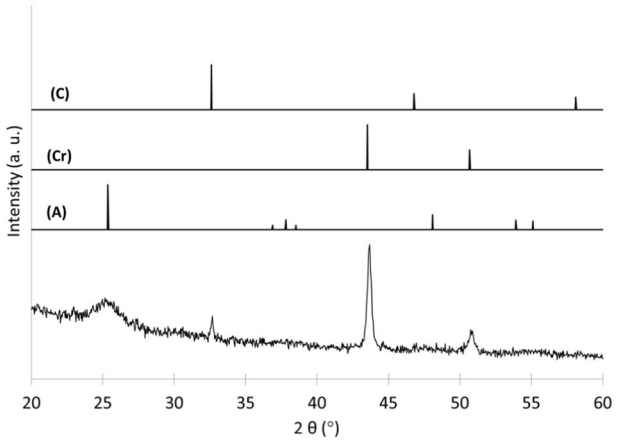

Fig. 5 Grazing incidence X-ray diffraction (GIXRD) pattern of the doped TiO_2 coating on brushed steel substrate. (A) Reference pattern of anatase, (Cr) Reference pattern of iron chromium carbide, and (C) Reference pattern of chromium oxide

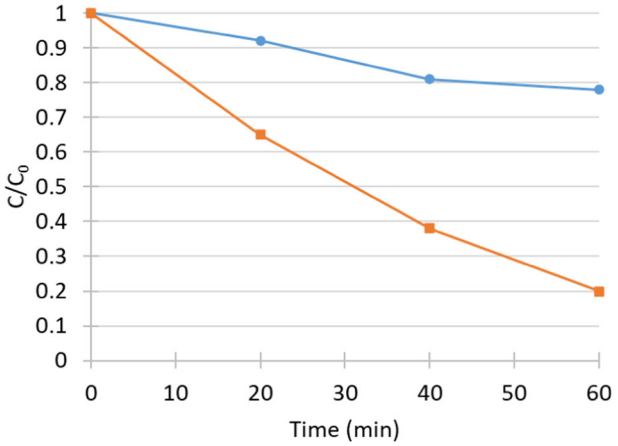

Fig. 6 RB degradation for (●) undoped TiO_2 and (■) doped TiO_2 films under LED light ($\lambda = 395$ nm) over time

previous section and used for the UVozone project. Indeed, this synthesis allowed crystalline TiO_2 material to be produced without calcination and used water as solvent. However, to be efficient under visible LED light, TiO_2 was co-doped with N and Fe, which have been previously identified as good dopants for visible-light applications [45]. The optimization of the composition was published in [45] and is not detailed here. The co-doped TiO_2 suspension (called doped TiO_2) is composed of anatase-brookite TiO_2 nanoparticle with 0.27 mol% of Fe and 0.5 mol% of N [45].

This suspension was deposited on brushed steel substrate using bar-coating. Figure 5 represents the XRD pattern of the coating. Anatase can be observed with the characteristic peak at 25°, while peaks of the steel substrate were also observed.

The thickness of the coating was not easy to evaluate as the substrate had a high roughness. Hence, mechanical profilometry was not possible on brushed steel but a similar deposition was made on glass for profilometry measurement. A thickness of 80 nm was measured on glass. The adherence of the coating was evaluated upon visual inspection with water, acetone and ethanol and no damage was observed.

To better evaluate the morphology of the samples, TEM and SEM images were taken on the pure and doped TiO_2. TEM pictures were obtained on the powder samples while the SEM images were taken of the coatings on steel substrate. These pictures are presented in Fig. S8. For both samples, the same morphology was observed corresponding to spherical nanoparticles of TiO_2 around 10 nm of diameter. SEM pictures also showed that a very rough surface was obtained at a nano level, providing substantial surface area for photocatalysis with these coatings. Indeed, no calcination step was done on the coating, to enable a very rough and porous surface to be retained (Fig. S8c, S8d).

To show the efficiency of the doping with Fe and N, the UV/visible diffuse reflectance of the doped TiO_2 powder is presented in Fig. S9 compared to the undoped aqueous TiO_2. A clear shift of the absorption spectrum towards the visible region was observed with a decrease in the band gap value from 2.9 eV to 2.65 eV.

The coating's photocatalytic activity was evaluated for RB degradation under LED illumination. Figure 6 represents the evolution of the degradation; a coating with undoped TiO_2 was also tested for comparison. The degradation was clearly enhanced by doping the TiO_2. For comparison, a coating made with a water suspension of Evonik P25 at the same concentration was produced; this latter coating has no activity under this visible LED illumination.

To achieve the ultimate goal of the project, the deposition method and the size of the substrate needed to be upscaled, as detailed in the next section.

3.2.3 Upscaled application

In order to cover larger substrates with a more industrial method, the coatings were produced by spray coating on brushed steel. Their photoactivity was evaluated on PNP degradation to verify that similar properties were maintained with the upscaled deposition method. Similar morphological features were obtained with all the up-scaled samples compared to the lab-sample deposited on steel (Fig. S8d).

First, deposition of the doped TiO_2 was made by spray-coating on brushed steel substrate of 75×25 mm in size. Two deposition parameters were studied: the dilution of the suspension to spray and the number of drying steps between the layer deposition. Indeed, to reach an effective thickness, several layers must be deposited. To obtain a good adherence and a visual uniformity of the surface, a dilution of the

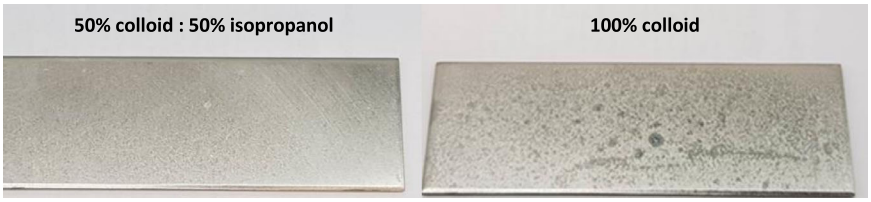

Fig. 7 Visual aspects of a doped TiO_2 coating with dilution (left) and without dilution (right)

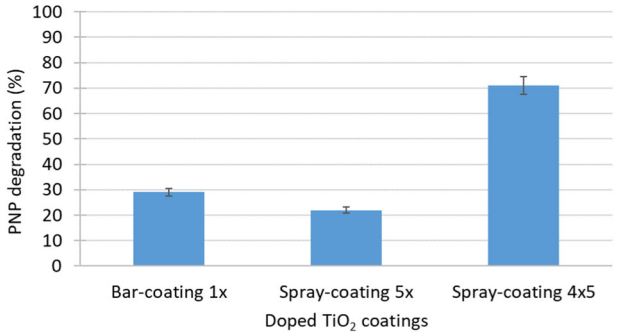

Fig. 8 *p*-Nitrophenol (PNP) degradation (%) for doped TiO_2 coatings in different deposition conditions under LED light ($\lambda = 395$ nm) after 24 h of illumination

suspension and a drying step between each five layers led to the best coating. As an example, Fig. 7 shows two coatings, one made with dilution and one without. It was clearly observed that the diluted suspension gives a homogeneous layer. Similar differences were observed between samples with and without intermediate drying steps.

Finally, the substrate was spray-coated using the dilute suspension and four deposition cycles. Each deposition cycle involved five spray-coating steps with washing and drying steps. This coating was tested on the degradation of PNP under LED illumination. The coating produced by bar-coating was also tested as a reference. Figure 8 shows the degradation after 24 h of reaction. It was observed that the degradation obtained by the spray-coating is 2.5 times better than that obtained by bar-coating.

In order to further increase the activity of the coating, a white painted layer was applied on steel before deposition of the doped TiO_2 layer to improve the reflection of the light. Substrates with 8 ×5 layers and 16 ×5 layers were also evaluated. The PNP degradation results for all substrates are summarized in Fig. 9 at 3 different times. It was observed that the sample with 16 ×5 layers deposited on the white painted steel gave the best degradation rate. The durability of the activity was also evaluated (Fig. 10) for these layers, with some activity being maintained after nine cycles of photocatalysis and a total of 58 h of illumination. When more layers were deposited, thicker, porous coatings (porous coatings as observed on SEM images, Fig. S8d) were obtained with higher photocatalytic efficiency (Fig. 9), due to the greater surface area in contact with the PNP.

In order to obtain a coated substrate that can be introduced in the pilot fountain, a larger surface needed to be covered. Substrates with a size of 250 × 150 mm were used with the same protocol as for the smaller slide (white painting sublayer and then 16 × 5 layers deposited). A homogeneous surface aspect was observed. Then, these plates were introduced in the pilot fountain, represented in Fig. 11. The coating was placed at the exit of the fountain as indicated by an arrow in Fig. 11. A more precise view of the fountain is presented in Fig. S10 with its exact dimensions.

This pilot fountain was then tested on model water polluted with RB (Fig. S7). After three days, the degradation reached 65%, showing the effectiveness of the global system at pilot scale. Moreover, no damage to the coating was observed and no Ti was detected in the water.

The optimized conditions (Table 2) to produce the most efficient visible photocatalytic coating involve deposition of the doped TiO_2 on 250 × 150 mm steel substrate via spray-coating with a white painting sublayer and then 16 × 5 layers deposited.

3.3 DAO project

3.3.1 Goal of the project

When depositing TiO_2 coatings, it is observed that the coating is hydrophilic. The goal of this project is to develop an easy-to-clean coating for steel for outdoor application. TiO_2 coating is a particularly good candidate as it produces hydrophilic coating with photocatalytic properties. This project will involve producing a layer at laboratory scale, evaluating its hydrophilic properties and then upscaling the synthesis to produce coatings on a classic roll-coating line used for steel to see if similar properties are obtained. The main development was published in [52].

3.3.2 Laboratory scale

A TiO_2 coating was deposited by bar-coating using the aqueous TiO_2 synthesis, since this approach allowed crystalline TiO_2 coatings to be produced without calcination and used water as solvent. The crystallinity of the corresponding powder was analyzed via XRD (Fig. 12), which revealed the presence of anatase and a small portion of brookite. The hydrophilicity of the coating was checked by water contact

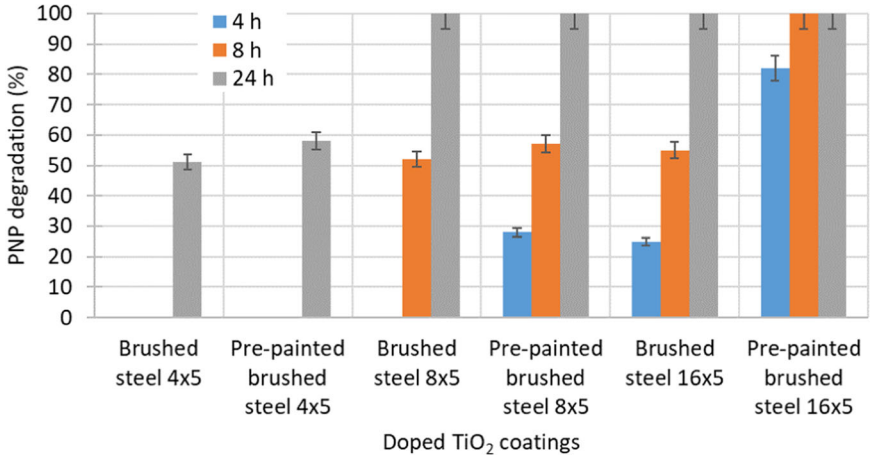

Fig. 9 *p*-Nitrophenol (PNP) degradation (%) for doped TiO_2 coatings with increased number of coating layer and with or without white painted sub-layer under LED light ($\lambda = 395$ nm) after 4, 8, and 24 h of illumination

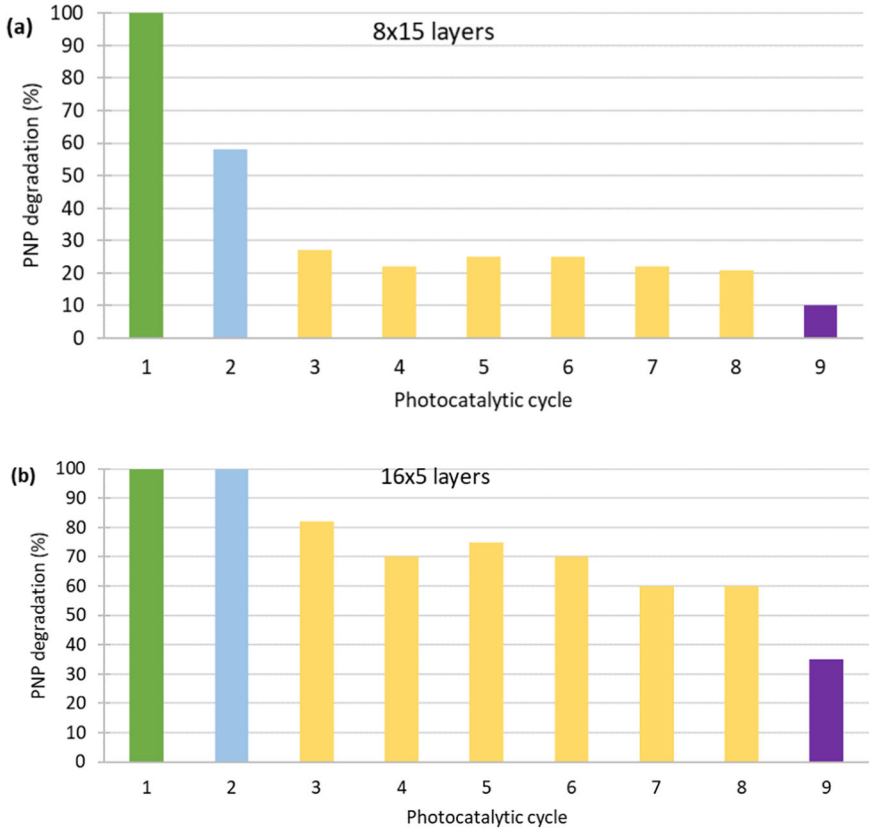

Fig. 10 *p*-Nitrophenol (PNP) degradation (%) for doped TiO_2 coatings with white painted sub-layer for (**a**) 8 x 5 layers sample and for (**b**) 16 x 5 layers sample with 9 successive photocatalytic cycles under LED light ($\lambda = 395$ nm). Each cycle can have a different duration depending on the inside color of the bars: green for 24 h, pale blue for 8 h, pale yellow for 4 h and purple for 2 h of illumination. After the 9 cycles, samples had undergone 58 h of photocatalytic experiment

angle measurement (Fig. 13); a comparison with the bare substrate is also shown. The adherence was also checked by visual inspection with water and ethanol. At laboratory scale, crystalline and hydrophilic coating of undoped TiO_2 was obtained.

3.3.3 Upscaled application

In order to deposit the coating using the pilot roll-coating line, a large volume of aqueous TiO_2 sol was needed. The synthesis was upscaled to a volume of 5 L (protocol in Large scale TiO_2 synthesis). To ensure that the large-scale synthesis was similar to that made in the laboratory, 20 mL of the large-scale suspension was dried under ambient air to obtain a TiO_2 powder. This powder was measured by XRD as shown in Fig. 12. A similar pattern to that obtained at laboratory scale was observed corresponding to anatase with a small fraction of brookite.

Then, 800×0.25 m of steel was covered by the TiO_2 coating. These coatings were then compared to those made on a laboratory scale. The water contact angle of the large-scale coating is shown in Fig. 13c; hydrophilic behavior

was observed compared to the bare substrate (Fig. 13a). Similar properties were obtained, showing the successful upscaling of both the synthesis and the deposition method [52].

The best conditions (Table 2) to obtain an efficient, easy-to-clean coating at large scale involve deposition of the aqueous TiO_2 at a speed of 60 m/min on steel surface previously treated with an acidic bath to increase the film adhesion.

4 Conclusions

In this work, throughout three different projects dealing with sol-gel TiO_2 coating, it was shown that upscaling laboratory results to pilot scale is possible. Indeed, each project leads to a larger scale application of the lab-scale developed product with similar efficiency.

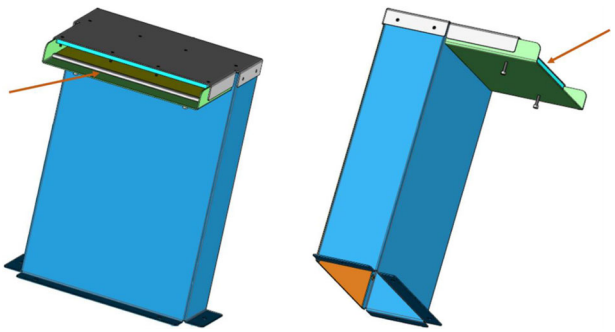

Fig. 11 Pilot fountain scheme in 3 dimensions. Orange arrows indicate the place where the photocatalytic steel plate is placed in the device

In the first project, the UV/Ozone project, a TiO_2 coating was developed to be deposited on the inside of a cylindrical reactor for water treatment. First at laboratory scale, two TiO_2 were successfully deposited on two different substrates: quartz and steel. These coatings were adherent, crystalline (anatase) and exhibited photoactivity for MB degradation. The aqueous TiO_2 synthesis was chosen for upscaling due to the possibility of depositing coatings without calcination and the use of water as solvent. On a larger scale, the inside of the steel reactor was covered by this aqueous TiO_2 coating. This reactor was efficient for MB degradation on a larger scale with no leaching of Ti. This project led to the commercialization of the reactor for swimming pool water treatment without chlorine.

In the second project, the BlueV project, a doped TiO_2 coating was developed to be photoactive under visible LED light. At laboratory scale, a doped TiO_2 coating was deposited on steel substrate using bar-coating. This crystalline anatase coating was shown to be efficient for the degradation of RB under LED light. Upscaling was conducted using a spray-coating technique and different protocols were tested and evaluated for the degradation of PNP under LED light. Finally, coating on larger, white-painted steel substrate (250 × 150 mm) was demonstrated, consisting of 16 x five layers deposited with drying and washing steps in-between. This coating allowed a PNP degradation of 80% after 4 h of illumination. This coated substrate was successfully introduced in a pilot fountain, showing photoactivity on model polluted water at large scale.

In the third project, the DAO project, an easy-to-clean coating for outdoor steel was developed. At laboratory scale, aqueous TiO_2 was deposited on steel and showed

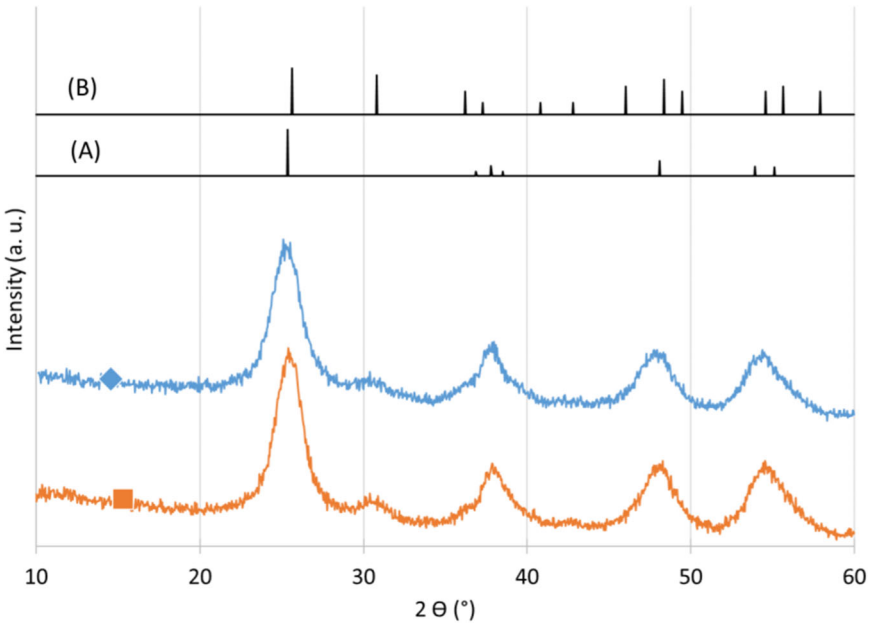

Fig. 12 X-Ray Diffraction (XRD) pattern of the undoped aqueous TiO_2 powder at (■) laboratory scale and (◆) large scale. (A) Reference pattern of anatase and (B) Reference pattern of brookite

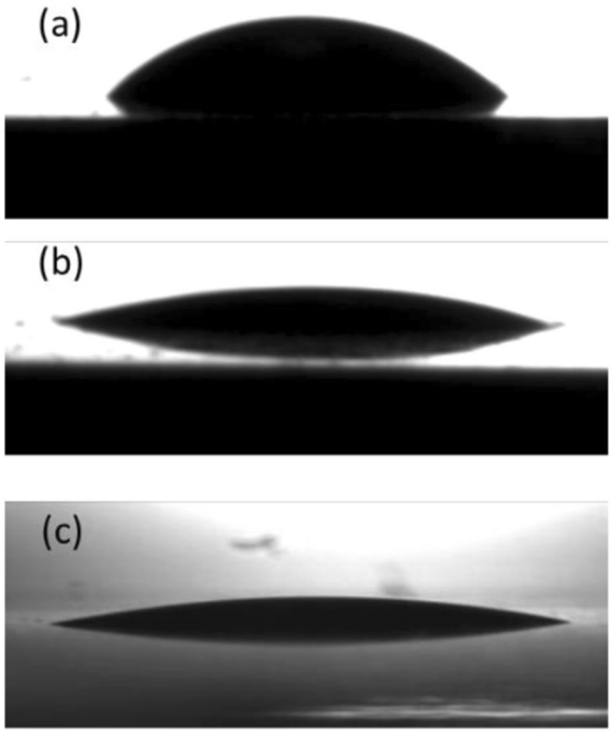

Fig. 13 Water contact angle (**a**) on bare steel, (**b**) on TiO_2 coated steel at lab-scale, and (**c**) on TiO_2 coated steel at large scale

anatase crystallinity and hydrophilicity. Larger scale synthesis of 5 L batches was successfully demonstrated with similar properties to those of the laboratory product. The large scale TiO_2 synthesis was deposited with a roll-coated pilot line on 800×0.25 m of steel. The upscaled product showed the same properties as the lab-scale product.

These developments demonstrate the possibility of bringing sol-gel TiO_2 products out of the laboratory towards pilot and industrial applications, and opens to ways for many possible up-scaled environmental applications.

Data availability

The raw/processed data required to reproduce these findings cannot be shared at this time as these data are part of an ongoing study.

Acknowledgements Julien G. Mahy and Stéphanie D. Lambert thank the F.R.S.-FNRS for their Postdoctoral Researcher position and Research Director position, respectively. The authors thank Isabelle Willems and Alain Germeau from Prayon S.A. for the provision of the extrapolation reactor. J.G.M. is grateful to the Rotary for a District 2160 grant, to the University of Liège and the FNRS for financial support for a postdoctoral stay in INRS Centre eau, terre, environnement in Québec, Canada.

Author contributions BH: Conceptualization, Methodology, Writing – review & editing, Investigation, Formal analysis, Writing – original draft, Funding acquisition, Project administration. SDL: Conceptualization, Methodology, Writing – review & editing, Formal analysis, Funding acquisition, Project administration. GL: Investigation, Formal analysis, Writing – review & editing. CA: Investigation, Formal analysis, Writing – review & editing. SD: Investigation, Formal analysis, Writing – review & editing. JC: Investigation, Formal analysis, Writing – review & editing. AD: Conceptualization, Funding acquisition, Project administration, Writing – review & editing. CA: Conceptualization, Funding acquisition, Project administration, Writing – review & editing. AD: Conceptualization, Funding acquisition, Project administration, Writing – review & editing. FL: Conceptualization, Methodology, Writing – review & editing, Supervision, Funding acquisition, Project administration. JGH: Conceptualization, Methodology, Writing – original draft, Writing – review & editing, Investigation, Formal analysis.

Funding Authors are grateful to the Département de la Recherche et du Développement technologique DGO6 of the Service Public de Wallonie and GreenWin, Competitivity Cluster of Wallonia, for financial support under Grant n°7744 (BlueV project). The authors are also grateful to the Ministère de la Région Wallonne Direction Générale des Technologies, de la Recherche et de l'Energie, in relation to the Plan Marshall, and with support from the Pôle MecaTech for the research project "DAO—Durable Aesthetic Outdoor Contract No. 6765."

Compliance with ethical standards

Conflict of interest The authors declare no competing interests.

Consent to participate All authors agreed to participate to this work.

Consent to publish All authors agreed to this version for publication.

Ethical approval The authors declare that they have no known competing financial interests or personal relationships that could have appeared to influence the work reported in this paper.

References

1. Brinker, CJ, Scherer GW (2013) Sol-gel science: the physics and chemistry of sol-gel processing. Academic press
2. Mahy JG, Deschamps F, Collard V et al. (2018) Acid acting as redispersing agent to form stable colloids from photoactive crystalline aqueous sol–gel TiO2 powder. J SolGel Sci Technol 87:568–583. https://doi.org/10.1007/s10971-018-4751-6
3. Claude V, Mahy JG, Geens J, Lambert SD (2019) Ni-doped γ-Al<inf>2</inf>O<inf>3</inf> as secondary catalyst for biosyngas purification: influence of Ni loading, catalyst preparation, and gas composition on catalytic activity. Mater Today Chem 13 https://doi.org/10.1016/j.mtchem.2019.05.002
4. Mahy JG, Tilkin RG, Douven S, Lambert SD (2019) TiO<inf>2</inf> nanocrystallites photocatalysts modified with metallic species: Comparison between Cu and Pt doping. Surfaces and Interfaces 17 https://doi.org/10.1016/j.surfin.2019.100366
5. Uchiyama H, Bando T, Kozuka H (2019) Effect of the amount of H2O and HNO3 in Ti(OC3H7i)4 solutions on the crystallization of sol-gel-derived TiO2 films. Thin Solid Films 669:157–161. https://doi.org/10.1016/j.tsf.2018.10.050
6. Haynes T, Hubert S, Carlier S, et al. (2020) Influence of water-miscible organic solvent on the activity and stability of silica-coated ru catalysts in the selective hydrolytic hydrogenation of cellobiose into sorbitol. Catalysts 10 https://doi.org/10.3390/catal10020149

7. Baranowska-Korczyc A, Mackiewicz E, Ranoszek-Soliwoda K, et al. (2022) Core/shell ag/sno2 nanowires for visible light photocatalysis. Catalysts 12 https://doi.org/10.3390/catal12010030
8. Mahy JG, Lejeune L, Haynes T, et al. (2021) Eco-friendly colloidal aqueous sol-gel process for tio2 synthesis: The peptization method to obtain crystalline and photoactive materials at low temperature. Catalysts 11
9. Mahy JG, Tasseroul L, Zubiaur A et al. (2014) Highly dispersed iron xerogel catalysts for p-nitrophenol degradation by photo-Fenton effects. Microporous Mesoporous Mater 197:164–173. https://doi.org/10.1016/j.micromeso.2014.06.009
10. Léonard GLM, Pirard SL, Belet A et al. (2019) Optimizing support properties of heterogeneous catalysts for the coupling of carbon dioxide with epoxides. Chem Eng J 371:719–729. https://doi.org/10.1016/j.cej.2019.04.055
11. Léonard GLM, Belet A, Grignard B et al. (2019) Heterogenization of a cyclocarbonation catalyst: Optimization and kinetic study. Catal Today 334:140–155. https://doi.org/10.1016/j.cattod.2018.11.060
12. Mahy JG, Claude V, Sacco L, Lambert SD (2017) Ethylene polymerization and hydrodechlorination of 1,2-dichloroethane mediated by nickel(II) covalently anchored to silica xerogels. J SolGel Sci Technol 81:59–68. https://doi.org/10.1007/s10971-016-4272-0
13. Guillén-Santiago, Mayén S, Torres-Delgado G et al. (2010) Photocatalytic degradation of methylene blue using undoped and Ag-doped TiO2 thin films deposited by a sol–gel process: Effect of the ageing time of the starting solution and the film thickness. Mater Sci Eng: B 174:84–87. https://doi.org/10.1016/j.mseb.2010.03.009. a. a.
14. Gratzel M (2001) Sol-gel processed TiO2 films for photovoltaic applications. J SolGel Sci Technol 22:7–13. https://doi.org/10.1023/A:1011273700573
15. Amirnasr M, Nazeeruddin MK, Grätzel M (2000) Thermal stability of cis-dithiocyanato(2,2′-bipyridyl4,4′dicarboxylate) ruthenium(II) photosensitizer in the free form and on nanocrystalline TiO2films. Thermochim Acta 348:105–114
16. Bodson CJ, Heinrichs B, Tasseroul L et al. (2016) Efficient P- and Ag-doped titania for the photocatalytic degradation of waste water organic pollutants. J Alloy Compd 682:144–153. https://doi.org/10.1016/j.jallcom.2016.04.295
17. Mahy JG, Tasseroul L, Herlitschke M et al. (2016) Fe3+/Iron Oxide/SiO2 Xerogel Catalysts for p-nitrophenol Degradation by Photo-Fenton Effects: Influence of Thermal Treatment on Catalysts Texture. Mater Today Proc 3:464–469. https://doi.org/10.1016/j.matpr.2016.01.043
18. Abbad S, Guergouri K, Gazaout S et al. (2020) Effect of silver doping on the photocatalytic activity of TiO2 nanopowders synthesized by the sol-gel route. J Environ Chem Eng 8:103718. https://doi.org/10.1016/j.jece.2020.103718
19. Al-Maliki FJ, Al-Lamey NH (2017) Synthesis of Tb-doped titanium dioxide nanostructures by sol–gel method for environmental photocatalysis applications. J SolGel Sci Technol 81:276–283. https://doi.org/10.1007/s10971-016-4190-1
20. Anderson C, Bard AJ (1995) An Improved Photocatalyst of TiO2/SiO2 Prepared by a Sol-Gel Synthesis. J Phys Chem 99:9882–9885. https://doi.org/10.1021/j100024a033
21. Ropero-Vega JL, Candal RJ, Pedraza-Avella JA et al. (2019) Enhanced visible light photoelectrochemical performance of β-Bi2O3-TiO2/ITO thin films prepared by aqueous sol-gel. J Solid State Electrochem 23:1757–1765. https://doi.org/10.1007/s10008-019-04270-0
22. Houmard M, Riassetto D, Roussel F et al. (2007) Morphology and natural wettability properties of sol-gel derived TiO2-SiO2 composite thin films. Appl Surf Sci 254:1405–1414. https://doi.org/10.1016/j.apsusc.2007.06.072
23. Tasseroul L, Pirard SL, Lambert SD et al. (2012) Kinetic study of p-nitrophenol photodegradation with modified TiO 2 xerogels. Chem Eng J 191:441–450. https://doi.org/10.1016/j.cej.2012.02.050
24. Benhebal H, Chaib M, Leonard A et al. (2012) Photodegradation of phenol and benzoic acid by sol-gel-synthesized alkali metal-doped ZnO. Mater Sci Semicond Process 15:264–269. https://doi.org/10.1016/j.mssp.2011.12.001
25. Hasnidawani JN, Azlina HN, Norita H et al. (2016) Synthesis of ZnO Nanostructures Using Sol-Gel Method. Procedia Chem 19:211–216. https://doi.org/10.1016/j.proche.2016.03.095
26. Mahy JG, Lejeune L, Haynes T, et al. (2021) Crystalline ZnO photocatalysts prepared at ambient temperature: Influence of morphology on p-nitrophenol degradation in water. Catalysts 11 https://doi.org/10.3390/catal11101182
27. Mahy JG, Mbognou MHT, Léonard C, et al. (2022) Natural Clay Modified with ZnO/TiO2 to Enhance Pollutant Removal from Water. Catalysts 12 https://doi.org/10.3390/catal12020148
28. Benhebal H, Wolfs C, Kadi S et al. (2019) Visible Light Sensitive SnO2/ZnCo2O4 Material for the Photocatalytic Removal of Organic Pollutants in Water. Inorg (Basel) 7:77
29. ben Haj Othmen W, Hamdi A, Addad A et al. (2018) Fe-doped SnO2 decorated reduced graphene oxide nanocomposite with enhanced visible light photocatalytic activity. J Photochem Photobio A Chem 367:145–155. https://doi.org/10.1016/j.jphotochem.2018.08.016
30. Benhebal H, Chaib M, Eonard AL, et al. (2013) Sol-gel preparation and characterisation of SnO2 powders employed as catalyst for phenol photodegradation. Scientia Iranica C 1891–1898
31. Páez CA, Liquet DY, Calberg C et al. (2011) Study of photocatalytic decomposition of hydrogen peroxide over ramsdellite-MnO2 by O2-pressure monitoring. Catal Commun 15:132–136. https://doi.org/10.1016/j.catcom.2011.08.025
32. Wu K, Wang Y, Zhitomirsky I (2010) Electrophoretic deposition of TiO2 and composite TiO2-MnO2 films using benzoic acid and phenolic molecules as charging additives. J Colloid Interface Sci 352:371–378. https://doi.org/10.1016/j.jcis.2010.08.059
33. Di Paola A, García-López E, Marcì G, Palmisano L (2012) A survey of photocatalytic materials for environmental remediation. J Hazard Mater 211–212:3–29. https://doi.org/10.1016/j.jhazmat.2011.11.050
34. Rauf MA, Ashraf SS (2009) Fundamental principles and application of heterogeneous photocatalytic degradation of dyes in solution. Chem Eng J 151:10–18. https://doi.org/10.1016/j.cej.2009.02.026
35. A Fujishima, Hashimoto K, Watanabe T (1999) TiO2 Photocatalysis: Fundamentals and Applications
36. Hoffmann MR, Martin ST, Choi Wonyong, Bahnemann DW (1995) Environmental Applications of Semiconductor Photocatalysis. Chem Rev 95:69–96. https://doi.org/10.1021/cr00033a004
37. Linsebigler AL, Lu Guangquan, Yates JT (1995) Photocatalysis on TiO2 Surfaces: Principles, Mechanisms, and Selected Results. Chem Rev 95:735–758. https://doi.org/10.1021/cr00035a013
38. Carp O (2004) Photoinduced reactivity of titanium dioxide. Prog Solid State Chem 32:33–177. https://doi.org/10.1016/j.progsolidstchem.2004.08.001
39. Pelaez M, Nolan NT, Pillai SC et al. (2012) A review on the visible light active titanium dioxide photocatalysts for environmental applications. Appl Catal B 125:331–349. https://doi.org/10.1016/j.apcatb.2012.05.036
40. Benkhennouche-Bouchene H, Mahy JG, Wolfs C et al. (2021) Green synthesis of N/Zr Co-doped TiO2 for photocatalytic degradation of p-nitrophenol in wastewater. Catalysts 11:1–21. https://doi.org/10.3390/catal11020235
41. Zaleska A (2008) Doped-TiO2: A Review. Recent Patents on Engineering 157–164

42. Delsouz Khaki MR, Shafeeyan MS, Raman AAA, Daud WMAW (2018) Evaluating the efficiency of nano-sized Cu doped TiO2/ZnO photocatalyst under visible light irradiation. J Mol Liq 258:354–365. https://doi.org/10.1016/j.molliq.2017.11.030
43. Pouretedal HR (2018) Visible photocatalytic activity of co-doped TiO2/Zr, N nanoparticles in wastewater treatment of nitrotoluene samples. J Alloy Compd 735:2507–2511. https://doi.org/10.1016/j.jallcom.2017.12.018
44. Mahy JG, Cerfontaine V, Poelman D, et al. (2018) Highly efficient low-temperature N-doped TiO2 catalysts for visible light photocatalytic applications. Materials 11 https://doi.org/10.3390/ma11040584
45. Douven S, Mahy JG, Wolfs C et al. (2020) Efficient N, Fe Co-Doped TiO2 Active under Cost-Effective Visible LED Light: From Powders to Films. Catalysts 10:547. https://doi.org/10.3390/catal10050547
46. Vo NQD, Huynh NDT, Huynh HT, et al. (2021) TiO2-SiO2 coatings onto cordierite honeycomb monolith support for effective photocatalytic degradation of β-naphthol in a water solution. Mater Lett 302 https://doi.org/10.1016/j.matlet.2021.130461
47. Guan K (2005) Relationship between photocatalytic activity, hydrophilicity and self-cleaning effect of TiO2/SiO2 films. Surf Coat Technol 191:155–160. https://doi.org/10.1016/j.surfcoat.2004.02.022
48. Manojkumar P, Lokeshkumar E, Saikiran A et al. (2020) Visible light photocatalytic activity of metal (Mo/V/W) doped porous TiO2 coating fabricated on Cp-Ti by plasma electrolytic oxidation. J Alloy Compd 825:154092. https://doi.org/10.1016/j.jallcom.2020.154092
49. Salvadores F, Minen RI, Carballada J et al. (2016) Kinetic Study of Acetaldehyde Degradation Applying Visible Light Photocatalysis. Chem Eng Technol 39:166–174. https://doi.org/10.1002/ceat.201500507
50. Paz Y (2010) Application of TiO2 photocatalysis for air treatment: Patents' overview. Appl Catal B 99:448–460. https://doi.org/10.1016/j.apcatb.2010.05.011
51. Jun TH, Lee K-S, Song HS (2012) Hydrophilicity of anatase TiO2/Cr-doped TiO2 thin films with different band gaps. Thin Solid Films 520:2609–2612. https://doi.org/10.1016/j.tsf.2011.11.026
52. Mahy JG, Léonard GL-M, Pirard S et al. (2017) Aqueous sol-gel synthesis and film deposition methods for the large-scale manufacture of coated steel with self-cleaning properties. J SolGel Sci Technol 81:27–35. https://doi.org/10.1007/s10971-016-4020-5
53. Malengreaux CM, Timmermans A, Pirard SL et al. (2012) Optimized deposition of TiO2 thin films produced by a non-aqueous sol–gel method and quantification of their photocatalytic activity. Chem Eng J 195–196:347–358. https://doi.org/10.1016/j.cej.2012.04.076
54. Crookes R (2007) Le décapage et la passivation de l' acier inoxydable. 4
55. Aquatic Science Notre histoire - Aquatic Science. https://www.aquatic-science.com/notre-histoire/. Accessed 21 Aug 2022